Vol. 706: 17–32, 2023
https://doi.org/10.3354/meps14256

MARINE ECOLOGY PROGRESS SERIES
Mar Ecol Prog Ser

Published February 23

Seasonal and interannual changes in a coastal Antarctic zooplankton community

John A. Conroy[1,*], Deborah K. Steinberg[1], Maya I. Thomas[1], Leigh T. West[1,2]

[1]Virginia Institute of Marine Science, William & Mary, Gloucester Point, VA, 23062, USA

[2]*Present address:* Center for Ecosystem Sentinels, Department of Biology, University of Washington, Seattle, WA, 98195, USA

ABSTRACT: Seasonal fluctuations are key features of high-latitude marine ecosystems, where zooplankton exhibit a wide array of adaptations within their life cycles. Repeated, sub-seasonal sampling of Antarctic zooplankton is rare, even along the West Antarctic Peninsula (WAP), where multidecadal changes in sea ice and phytoplankton are well documented. We quantified zooplankton biomass, size structure, and composition at 2 coastal time-series stations in the northern WAP over 3 field seasons (November–March) with different sea-ice, temperature, and phytoplankton conditions. Seasonal peaks in zooplankton biomass followed weeks after phytoplankton blooms. Biomass of mesozooplankton (0.2–2 mm) was consistent and low, while high biomass of macrozooplankton (>2 mm) occasionally resulted in a size distribution dominated by krill and salps, which appears to be a characteristic phenomenon of the Southern Ocean. Zooplankton composition and size changed between years and from spring to summer as the water column warmed after sea-ice breakup. Seasonal succession was apparent typically in decreasing zooplankton size and a shift to species that are less dependent upon phytoplankton. Mean central abundance dates varied by 54 d across 14 taxa, and specific feeding preferences and life-history traits explained the different seasonal abundance patterns. In all 3 yr, the dominant euphausiid species switched from *Euphausia superba* in spring to *Thysanoessa macrura* in late summer. Various taxa shifted their phenology between years in response to the timing of sea-ice breakup and the onset of phytoplankton productivity, a level of natural environmental variability to which they appear resilient. Nevertheless, the limits to this resilience in response to climate change remain uncertain.

KEY WORDS: Phenology · Succession · Biomass · Copepod · Krill · Salp · Pteropod · Southern Ocean

1. INTRODUCTION

The seasonal timing of zooplankton migration, reproduction, and growth is coupled with annual cycles of prey availability and temperature throughout the global ocean (Ji et al. 2010). As a consequence, seasonal patterns of zooplankton biomass and abundance change from year to year (Mackas et al. 2012). These cycles are particularly pronounced in high-latitude ecosystems, where zooplankton employ a range of life-history strategies that vary with body size, trophic level, and life span (Visser et al. 2020). The West Antarctic Peninsula (WAP) is one such seasonally productive ecosystem that has undergone considerable physical and ecological change over recent decades (Henley et al. 2019). While coastal time-series programs document the sub-seasonal drivers and variability of physical conditions, chemical stocks, and phytoplankton along the WAP since the 1990s (Kim et al. 2016, 2018), such data are scarce for zooplankton.

Limited prior results from sampling on the scale of weeks to months demonstrate the impact of temperature, sea-ice coverage, and phytoplankton biomass

*Corresponding author: jaconroy@vims.edu

Publisher: Inter-Research · www.int-res.com

on zooplankton growth, reproduction, and distribution in the Southern Ocean. Past work focused on individual macrozooplankton species, such as the Antarctic krill *Euphausia superba* (Bernard et al. 2017, Nardelli et al. 2021), the salp *Salpa thompsoni* (Loeb & Santora 2012, Groeneveld et al. 2020), and the pteropod *Limacina rangii* (Thibodeau et al. 2020), the currently recognized name (Janssen et al. 2019) for the species previously called *Limacina helicina antarctica*. While seasonal shifts in abundance, vertical distribution, and species composition have been described for copepod assemblages in the Southern Ocean (Atkinson 1998, Schnack-Schiel 2001), community-wide (multi-taxa) zooplankton studies with sub-seasonal resolution are particularly rare (Froneman et al. 1997, Hunt & Hosie 2006). Climate-induced phenology shifts may increase the likelihood of seasonal trophic mismatches between zooplankton and phytoplankton (Richardson 2008, Thackeray et al. 2016), but data limitation hinders the assessment of zooplankton phenology and seasonal succession in the Southern Ocean.

In addition to taxonomy, zooplankton composition and seasonal succession can be related to organismal traits (Litchman et al. 2013, Kiørboe et al. 2018). Size is a key trait that governs an individual's metabolic rate and also has consequences for ecosystem-level processes such as particle export (Brown et al. 2004, Stamieszkin et al. 2015). Different feeding modes are favored during different periods of the annual cycle, resulting in seasonal shifts in both zooplankton and prey (Kenitz et al. 2017). Survival traits (e.g. seasonal vertical migration) and reproductive traits (e.g. spawn timing) are particularly important in high-latitude environments, where zooplankton adapt a range of strategies to endure winter (Visser et al. 2020). These traits provide a useful perspective for interpreting seasonal patterns across the broad range of taxonomic groups that comprise zooplankton assemblages.

To address the above knowledge gaps, we analyzed zooplankton biomass and the abundance of major taxa at 2 coastal time-series stations as part of the Palmer Antarctica Long-Term Ecological Research (PAL LTER) program. Net sampling was conducted twice per week across 3 consecutive field seasons to examine changes in spring–summer zooplankton composition. We hypothesized that environmental conditions (e.g. phytoplankton biomass and temperature) impact zooplankton biomass and composition at seasonal to interannual scales. Our approach sought to reveal patterns of taxonomic and trait-based succession not previously resolved for zooplankton in this pelagic marine ecosystem.

2. MATERIALS AND METHODS

2.1. Zooplankton collection

Daytime sampling trips from Palmer Station (64° 46′ S, 64° 03′ W) were conducted aboard a rigid-hulled inflatable boat during 3 consecutive field seasons spanning austral spring to late summer: 17 November 2017 to 12 March 2018, 6 November 2018 to 11 March 2019, and 6 January 2020 to 2 March 2020. Macro- and mesozooplankton were collected twice weekly, as weather permitted, southwest of Anvers Island, Antarctica, at PAL LTER Stations B and E, respectively located ~1 and ~5 km from Palmer Station (Fig. 1). The bottom depth is ~70 m at Station B and ~160 m at Station E, which is northeast of the Palmer Deep canyon. Station E was sampled before Station B each

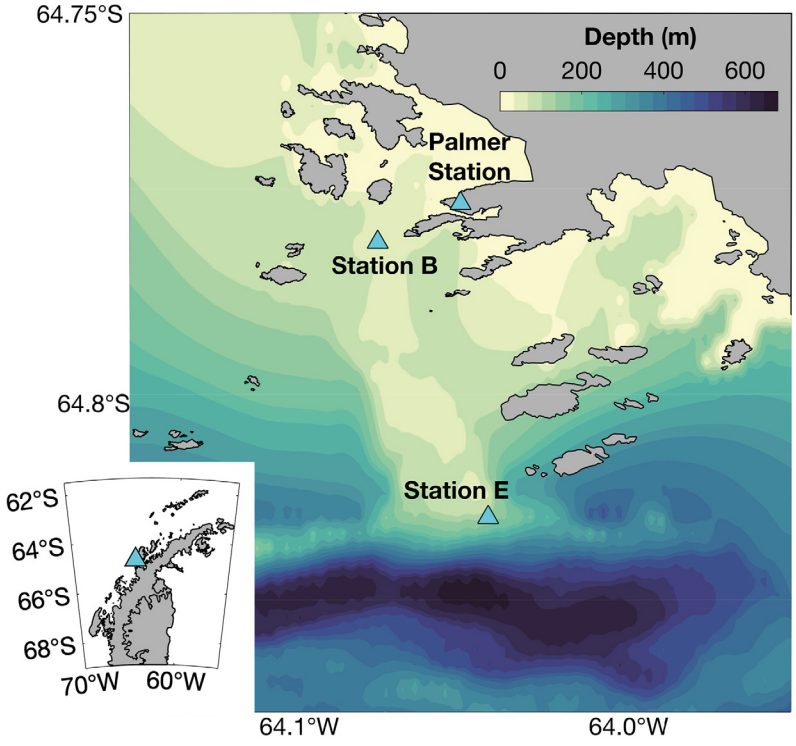

Fig. 1. Study area indicating time-series Stations B (~70 m depth) and E (~160 m depth) near Palmer Station on Anvers Island, Antarctica. The triangle in the inset map marks the location of the study area along the West Antarctic Peninsula

day, and tows were usually conducted between 10:00 and 15:00 h local time. Sampling 2 stations allowed the assessment of differences between a nearshore site and a canyon edge location while also improving sampling effectiveness for patchily distributed zooplankton.

Zooplankton were collected using 2 net types: a 1 × 1 m square, 700 µm mesh Metro net and a 1 m diameter, 200 µm mesh ring net, which were both towed obliquely to a target depth of 50 m. Wire payout and retrieval rate was ~23 m min^{-1}. Speed over ground was ~2.0 knots while towing the 700 µm net and ~1.5 knots while towing the 200 µm net. Duplicate tows were typically conducted with each net at both sampling stations. A General Oceanics flow meter was used to determine the volume of water filtered (= 407 ± 106 m^3 [mean ± SD] for the 700 µm net; 197 ± 84 m^3 for the 200 µm net). Due to a flowmeter malfunction, volume filtered was unavailable for twelve 200 µm net tows in January 2020. Estimated values were calculated from a polynomial regression fit of volume filtered vs. the length of wire out ($y = -0.0664x^2 + 14.6x - 603$; $p < 0.04$ for all parameters; $R^2 = 0.84$). Maximum net depth was estimated during each tow based on the length and angle of wire out and verified using a Star-Oddi DST centi-TD (50 ± 4 m [mean ± SD] for the 700 µm net; 50 ± 7 m for the 200 µm net).

2.2. Zooplankton analysis

The Metro and ring nets were used to quantify different taxa. Both replicate tows with the 700 µm net were assessed for taxonomic composition, and data are presented for the following taxa: euphausiids (krill) *Euphausia superba* and *Thysanoessa macrura*, the thecosome (shelled) pteropod *Limacina rangii*, gymnosome (un-shelled) pteropods (including *Clione limacina* and *Spongiobranchaea australis*), the salp *Salpa thompsoni* (individuals of the blastozooid life stage >3 mm and oozooid life stage >10 mm), amphipods, and larval fishes. These taxa dominated biomass and were sorted live and counted in the aquarium room at Palmer Station. On rare occasions when subsampling was necessary, a random subsample containing at least 100 individuals of the abundant taxon was taken by stirring the sample to homogenize it and subsampling with an aquarium net. The proportion of the subsample was calculated using displacement biovolume. On 4 dates between 15 February 2020 and 2 March 2020, sampling was restricted to the 700 µm net, and only Station E was sampled. Only salps and euphausiids were quantified from the 8 tows conducted during that date range.

One of the 200 µm net samples from each station was used for taxonomic analysis, and data are presented for the following taxa: copepods *Oithona* spp., *Calanoides acutus* (>1 mm only), *Calanus propinquus* (>1 mm only), *Rhincalanus gigas* (>1 mm only), and small calanoids (0.2–1 mm), chaetognaths, asteroid larvae (bipinnaria and brachiolaria stages), and nemertean pilidium larvae. The >1 mm limit for calanoid copepod species ensured consistent classification across analysts. Globigerinid foraminifera data were limited and thus were only analyzed to test an observed association with sea ice. The samples were preserved in 3.7% formaldehyde buffered with sodium borate. Then they were returned to the Virginia Institute of Marine Science (Gloucester Point, Virginia, USA) for further microscopic enumeration. Preserved samples were size-fractionated with nested sieves into the following 5 size classes: 0.2–0.5, 0.5–1, 1–2, 2–5, and >5 mm. All individuals in the 3 largest size fractions were typically identified and counted. Typically, at least 1/64 of the 2 smallest size fractions was counted under a stereo dissecting microscope after dividing the sample with a Folsom plankton splitter. Size fractions were split such that at least 100 individuals of the most abundant taxon were present (Postel et al. 2000).

The second 200 µm net sample from each station was split in half with a Folsom plankton splitter immediately upon collection. One-half of the catch was processed and flash frozen on board the rigid-hulled inflatable boat for future analysis. Upon return to Palmer Station, the second half of the catch was size-fractionated with nested sieves (into the same size classes as above), concentrated on preweighed 200 µm mesh filters, and frozen at −20°C. Samples were thawed, weighed to determine wet biomass, dried at 60°C for at least 24 h, and weighed again to determine dry biomass. Zooplankton dry weight density (g m^{-3}) was then depth-integrated to 50 m (g m^{-2}).

2.3. Environmental data

Due to the localized nature of sea-ice dynamics, the date of the first CTD cast at Palmer Station was used to demarcate local sea-ice breakup. In all 3 yr, small-boat operations were delayed until sea-ice concentration declined to ~50%. Satellite-based data provided a broader spatial and multi-decadal context for the date of sea-ice retreat. The satellite-based

date of sea-ice retreat was calculated from daily sea-ice concentration for the 50 × 50 km area south and west of Anvers Island using the Bootstrap passive microwave algorithm (version 3.1) (Stammerjohn et al. 2008, Schofield et al. 2017). The date of retreat was defined as the final day for which sea-ice concentration remained above 15% for 5 consecutive days. Local ice coverage within a radius of ~400 m was also recorded at the start of each net tow using a scale of 10% increments.

PAL LTER Stations B and E were usually sampled for water column properties on the mornings of zooplankton collections (Schofield et al. 2017). CTD (SeaBird Electronics Seacat SBE 19plus sensor) casts sampled to depths of 60 and 75 m at Stations B and E, respectively. Data from downcast profiles were averaged in 1 m bins. The average temperature (T) and maximum temperature (T_{max}) in the upper 50 m were calculated for each cast. Discrete water samples for fluorometric chlorophyll *a* (chl *a*) analysis were collected in Niskin bottles at 7 depths on the upcast, filtered onto Whatman GF/F filters, and frozen at −80°C. Samples were extracted in 90% acetone at −20°C for 24 h and analyzed with a Turner 10AU fluorometer. Chl *a* profiles were depth-integrated to 50 m. Sampling coverage was greater for these environmental variables than for zooplankton collection across all 3 field seasons and spanned the following date ranges: 14 November 2017 to 26 March 2018, 2 November 2018 to 28 March 2019, and 2 December 2019 to 19 March 2020.

The coast near Palmer Station experiences a mixed tide, fluctuating between several days of semidiurnal tide (i.e. 2 high and 2 low tides each day) and several days of diurnal tide (i.e. 1 high and 1 low tide each day) (Amos 1993). The tidal regime (more than the daily tidal oscillations) influences surface current direction, nearshore distribution of *E. superba*, and the foraging range of Adélie penguins (Oliver et al. 2013, Bernard et al. 2017). Tide height data at 1 min intervals were obtained from the Palmer Station tide gauge via the Antarctic Meteorological Research Center (https://amrc.ssec.wisc.edu/usap/palmer/). The tidal regime for each sampling day was manually classified as diurnal or semidiurnal tide based on the number of maxima and minima in tide level.

2.4. Data analysis

We tested whether zooplankton dry weight, taxon abundance, chl *a*, average T, and T_{max} differed between Stations B and E across the 3 field seasons using the Wilcoxon signed-rank test. This paired, non-parametric test does not assume that data are normally distributed. The Kruskal-Wallis 1-way ANOVA was used to test whether zooplankton dry weight, chl *a*, average T, and T_{max} each differed between years. Individual year-to-year comparisons were performed using Dunn's test on rank sums with a Bonferroni correction. Spearman's rank correlation was used to test an observed connection between foraminifera and local sea-ice coverage. These analyses were conducted using R version 4.0.5 (R Core Team 2021). Dunn's test was executed using the 'dunn.test' package (version 1.3.5) in R (Dinno 2017).

Variation in zooplankton size structure was analyzed by plotting normalized biomass size spectra. Normalized biomass was calculated as dry weight density divided by the size interval of a given size fraction (i.e. 0.3, 0.5, 1, 3, or 5 mm) (Rykaczewski & Checkley 2008). Visual inspection revealed that the larger size fractions (>2 mm) often contributed relatively high biomass, making it inappropriate to calculate spectral slope from a linear best-fit line. Thus, samples were divided into low (<0.03 g m^{-2}; n = 34 samples), medium (0.03–0.1 g m^{-2}; n = 46), and high (>0.1 g m^{-2}; n = 36) zooplankton biomass conditions to allow comparison of the size spectra as a function of total biomass.

A multivariate analysis of the abundance data for 15 taxa was conducted to assess change in taxonomic composition. Foraminifera (due to inconsistent quantification) and oozooids of *S. thompsoni* (due to scarcity relative to blastozooids) were excluded from this analysis; blastozooids of *S. thompsoni* were included. This analysis was conducted using the 'vegan' package (version 2.5-7) in R (Oksanen et al. 2020). When duplicate tows were conducted, the mean of species abundance was used. ANOSIM using the Bray-Curtis dissimilarity and 10 000 permutations tested whether community structure differed significantly between years and between Stations B and E. Non-metric multidimensional scaling (NMDS) was used to visualize the similarity of sampling dates within a given year. NMDS is an ordination technique that reduces a multidimensional dataset into a smaller number of dimensions so that similar samples are located closer to one another (Minchin 1987). NMDS using the Bray-Curtis dissimilarity matrix is able to accommodate zeroes and skewed data. NMDS was executed with the function 'metaMDS' using a square-root transformation and Wisconsin double standardization. NMDS ordination solutions for the 2017–2018 and 2019–2020 field seasons converged

using 2 dimensions, but 3 dimensions were required for the 2018–2019 field season.

Linear regression analysis on the annual NMDS ordinations was used to identify the directional gradients of environmental variables hypothesized to impact zooplankton composition (e.g. Dietrich et al. 2021). Days since local sea-ice breakup (based on first day of boat-based sampling) was used to examine the seasonal progression of each year. Average *T* and chl *a* are commonly related to zooplankton life-history processes (chl *a* was $\log_{10}$-transformed) (e.g. Mackas et al. 2012, Atkinson et al. 2015). Tidal regime was hypothesized to impact zooplankton composition, because it influences local surface currents (Oliver et al. 2013, Bernard et al. 2017). The resulting vectors indicate the direction of maximal change for a given environmental variable, and the r^2 statistic indicates the correlation strength along a vector's axis. This regression analysis was conducted with the 'envfit' function of 'vegan' using 10 000 permutations.

The central date of zooplankton density was calculated using a 'center of gravity' metric for individual biomass size classes and for abundances of 14 taxa (Edwards & Richardson 2004, Mackas et al. 2012). Foraminifera (due to inconsistent quantification) and both stages of *S. thompsoni* (due to scarcity) were excluded from this analysis. For this calculation, dates were numbered sequentially beginning with 1 November. The central date for a given size-fraction or taxon was calculated as the sum of the products of daily densities (N_D) and sampled day numbers (D), divided by the sum of daily densities: $\sum N_D \times D / \sum N_D$. Only data collected from 5 December to 12 March were included, as this period was consistently sampled during the 2017–2018 and 2018–2019 field seasons. The 2019–2020 field season was excluded due to limited sampling coverage. Central dates were calculated individually for Stations B and E. In cases of bimodal distributions, the central date calculated using this method falls between 2 peaks.

3. RESULTS

3.1. Sea ice and temperature

The date of local sea-ice breakup varied by 4 wk across the 3 field seasons: 16 November 2017, 2 November 2018, and 29 November 2019 (Fig. 2). This interannual pattern in local sea-ice breakup (mid-, early-, and later-season, respectively) corresponds with satellite observations indicating sea-ice retreat dates of 26 November 2017, 23 November 2018, and 7 December 2019 for the area 50 km south and west of Anvers Island.

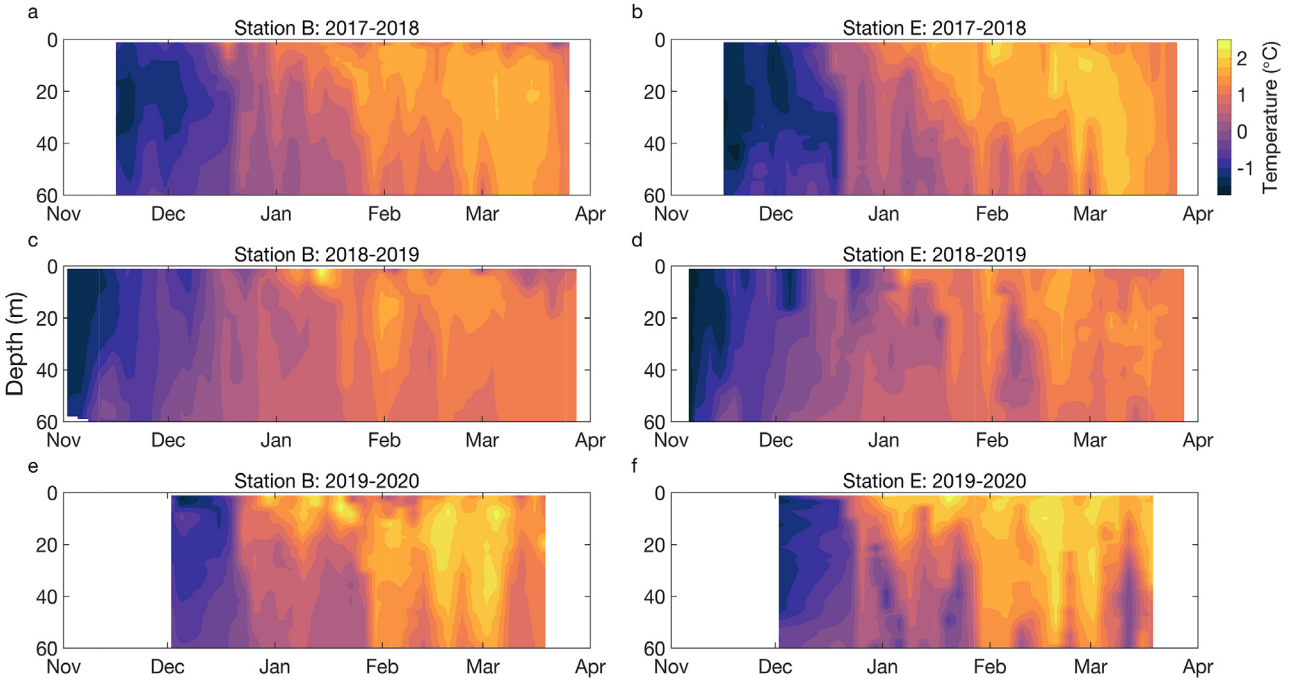

Fig. 2. Temperature time series from (a, c, e) Station B and (b, d, f) Station E during the (a,b) 2017–2018, (c,d) 2018–2019, and (e,f) 2019–2020 field seasons. Vertical temperature profiles (collected twice per week) were interpolated to produce section plots. Time series begin at the first date local sea-ice breakup allowed boat-based water sampling from Palmer Station

Water temperature in the upper 50 m (range: −1.7°C to 2.5°C) warmed throughout each field season and differed substantially among years. Average T and T_{max} did not differ between Stations B and E (Wilcoxon signed-rank tests: $p > 0.15$ for both tests; n = 106 sample pairs). Winter water ($T \leq -1.2$°C) persisted until ~10 December regardless of the timing of local sea-ice breakup (Fig. 2). From mid-December onwards, the water column generally warmed from the surface through depth. During the summer period of 26 December to 21 March, average T and T_{max} differed significantly across years (Kruskal-Wallis test: average T, $\chi^2 = 17$, df = 2, $p < 0.001$; T_{max}, $\chi^2 = 69$, df = 2, $p < 0.0001$). Average T was colder in 2018–2019 than in the other 2 yr (Dunn's test: $p < 0.001$ for both comparisons), while T_{max} was significantly different across all years, being warmest in 2019–2020 and coldest in 2018–2019 (Dunn's test: $p < 0.001$ for all comparisons) (Table 1).

3.2. Phytoplankton biomass

The timing and magnitude of phytoplankton accumulation changed across field seasons and was related to the timing of local sea-ice breakup. Chl *a* concentration did not differ between Stations B and E (Wilcoxon signed-rank test: $p = 0.065$; n = 106 sample pairs). Chl *a* was low upon sea-ice breakup, then increased over the following 2–3 wk to a peak typically exceeding 200 mg m^{-2} (Fig. 3). Regardless of initial bloom timing, chl *a* remained relatively high until dropping below 50 mg m^{-2} in January, then increasing above 60 mg m^{-2} in late January and early February each year. A final chl *a* peak (>100 mg m^{-2}) occurred in March of each year. Despite similar seasonal patterns, chl *a* differed significantly between years (Kruskal-Wallis test: $\chi^2 = 9.7$; df = 2; $p = 0.008$) and was higher in 2018–2019 than in 2017–2018 or 2019–2020 (Dunn's test: $p = 0.01$ for both comparisons) (Table 1).

3.3. Zooplankton biomass and size composition

Similar to chl *a*, zooplankton dry weight (range: 0.007 to 3.0 g m^{-2}) and seasonal patterns differed among years. Dry weight did not differ between Stations B and E (Wilcoxon signed-rank test: $p = 0.88$; n = 50 sample pairs). Zooplankton biomass maxima in December 2017 and January 2018 occurred 2–3 wk after chl *a* peaks (Fig. 3a,b). Zooplankton and phytoplankton biomass then both remained low in late February and March 2018 (Fig. 3a,b). The following year was characterized by zooplankton biomass peaks in December and February also following phytoplankton peaks (Fig. 3c,d). Zooplankton biomass was higher in 2020 than in the other 2 field seasons (Kruskal-Wallis test: $\chi^2 = 27.4$; df = 2; $p < 0.0001$; Dunn's test: $p < 0.0001$ for both comparisons) (Table 1), and elevated biomass in January followed a phytoplankton peak in late December (Fig. 3e,f).

Zooplankton biomass dynamics were linked to size structure, which changed on seasonal and annual time scales. Comparing the size spectra for low, medium, and high biomass conditions revealed that mesozooplankton (0.2–2 mm) formed a relatively consistent background biomass (Fig. 4). Increased total biomass was due to higher abundance of macrozooplankton (>2 mm), with the largest size class (>5 mm) in particular driving the highest biomass conditions. Decreasing size from December 2017 to March 2018 was consistent with decreasing biomass late in that field season as the smallest (0.2–0.5 mm) size class proportionally replaced the largest size class (Fig. 5a). High biomass and dominance of >5 mm animals again characterized December 2018, and a large contribution of animals >2 mm drove the second biomass peak in late summer (Fig. 5b). On average, >5 mm animals constituted 82% of dry weight in 2020 when the highest biomass was observed (Fig. 5c). Across years, the smallest (0.2–0.5 mm) size class consistently dominated when animals >2 mm were scarce. The intermediate sizes (0.5–1 mm and 1–2 mm) typically constituted <20% of total zooplankton biomass.

Table 1. Summary statistics of water temperature and plankton biomass variables for each field season at Palmer Station. Temperature observations (0–50 m) only include sampling between 26 December and 21 March. Chlorophyll *a* and zooplankton dry weight (integrated from 0–50 m) include all sampling dates. Data from Stations B and E are included

Field season	Average temp. (°C)		T_{max} (°C)		Chl *a* (mg m^{-2})		Zooplankton dry weight (g m^{-2})	
	Mean ± SD	n	Mean ± SD	n	Mean ± SD	n	Mean ± SD	n
2017–2018	1.2 ± 0.46	49	1.6 ± 0.34	49	67 ± 38	76	0.15 ± 0.30	40
2018–2019	0.95 ± 0.32	50	1.3 ± 0.34	50	96 ± 77	84	0.093 ± 0.16	60
2019–2020	1.3 ± 0.47	50	1.9 ± 0.32	50	69 ± 54	58	0.92 ± 0.79	16

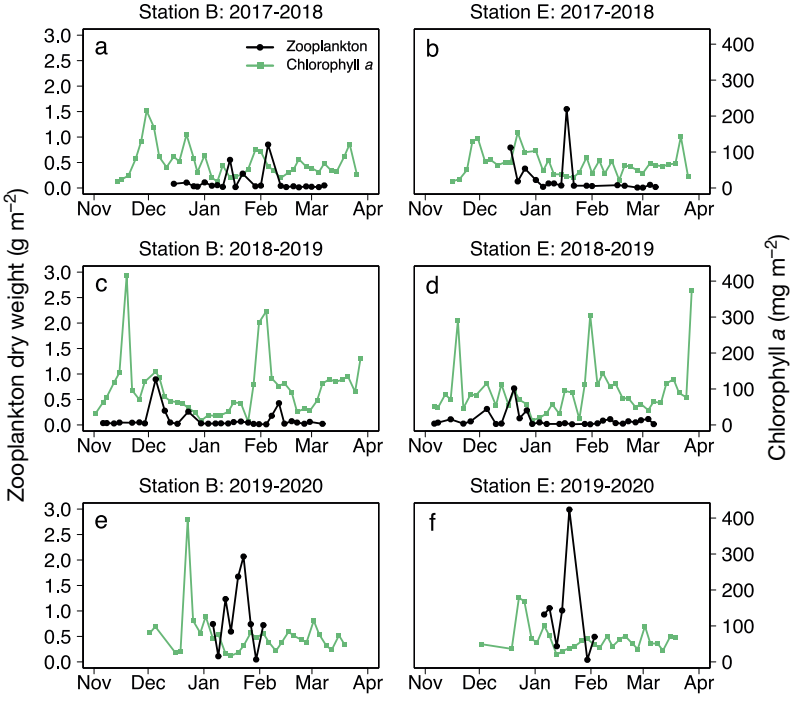

Fig. 3. Chl *a* and zooplankton dry weight time series from (a,c,e) Station B and (b,d,f) Station E during the (a,b) 2017–2018, (c,d) 2018–2019, and (e,f) 2019–2020 field seasons. Both variables were integrated from 0 to 50 m

3.4. Zooplankton taxonomic composition and seasonal patterns

Multivariate analysis of 15 taxa revealed interannual and seasonal changes in zooplankton composition. Taxonomic composition differed significantly among years (ANOSIM: R = 0.16; p < 0.001) and between sampling stations (ANOSIM: R = 0.11; p < 0.001). NMDS scores illustrated seasonal succession and were significantly correlated with the number of days since sea-ice breakup in all years (Fig. 6 & Fig. S1 in the Supplement at www.int-res.com/articles/suppl/m706p017_supp.pdf, Table 2). Average *T* was significantly correlated with the ordination scores for 2017–2018 and 2018–2019. Chl *a* and tidal regime were not significantly correlated with NMDS scores (Table 2).

Central abundance dates captured the seasonal succession in zooplankton taxonomic and size class composition (Fig. 7). The earliest mean central abundance dates were for *Euphausia superba* and pteropods, while *Thysanoessa macrura* and the copepods *Calanus propinquus* and *Oithona* spp. were the latest taxa (Fig. 7a). In 2017–2018 and 2018–2019, *E. superba* dominated the >5 mm size class, which had the earliest mean central biomass date (Fig. 7b). Similarly, *Oithona* spp. and *T. macrura* dominated the 0.2–0.5 and 2–5 mm size classes, respectively, which were the latest size classes to appear.

The seasonal succession in euphausiid species was apparent in all 3 yr. Although *T. macrura* was more abundant at Station E (Table 3), daily mean density for both euphausiid species was calculated using Stations B and E combined due to frequent absence on a given sampling event. Mean density of *E. superba* was highest in November and December, with seasonal declines beginning in January (Fig. 8). *T. macrura* was always less abundant than *E. superba* during November and December but was always more abundant by March. The central abundance date for *E. superba* was 65 and 57 d earlier than that of *T. macrura* in 2017–2018 and 2018–2019, respectively (Fig. 8a,b).

Several taxa were more abundant at Station B than at Station E (Table 3), and their different seasonal abundance patterns resulted in succession among groups. Larval fishes, *C. acutus*, and small calanoid copepods typically increased rapidly following sea-ice breakup (Fig. S2 in the Supplement), and their mean central abundance dates ranged from 11–13 January (Fig. 7a). Amphipods, larval asteroids, and larval ne-

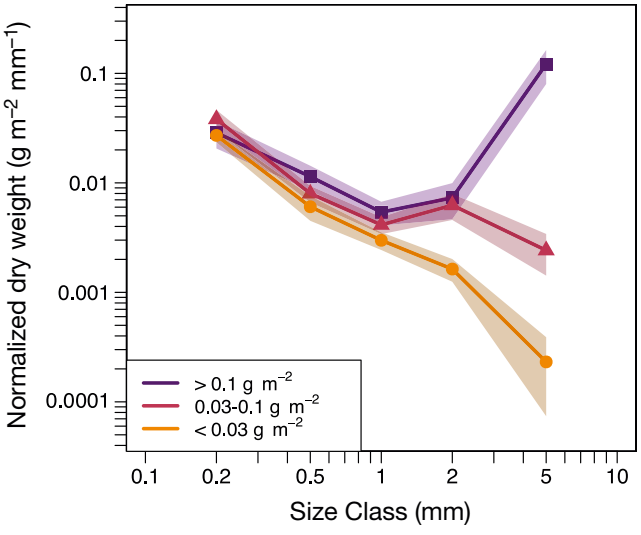

Fig. 4. Mean normalized zooplankton biomass size spectra as a function of total dry weight density. Data were divided into 3 categories with similar sample size based on the total dry weight density integrated from 0 to 50 m (n = 34–46 samples per point). Shading indicates ±2 SE

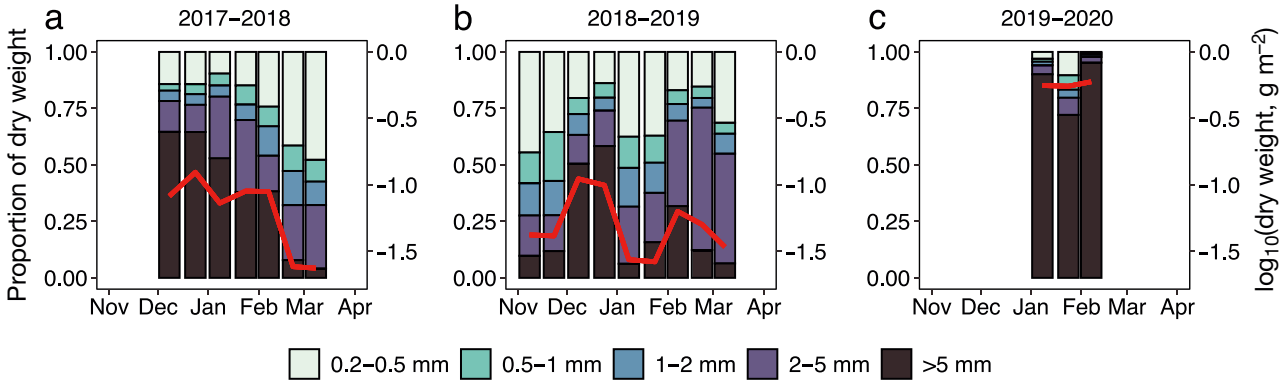

Fig. 5. Time series of zooplankton size composition and biomass during the (a) 2017–2018, (b) 2018–2019, and (c) 2019-2020 field seasons. Stacked bar charts indicate the mean proportional contribution of 5 zooplankton size classes to the total dry weight in each 2 wk period, and the red line indicates mean $\log_{10}$-transformed zooplankton dry weight density integrated from 0 to 50 m (n = 1–10 samples per 2 wk period). Data from Stations B and E are combined

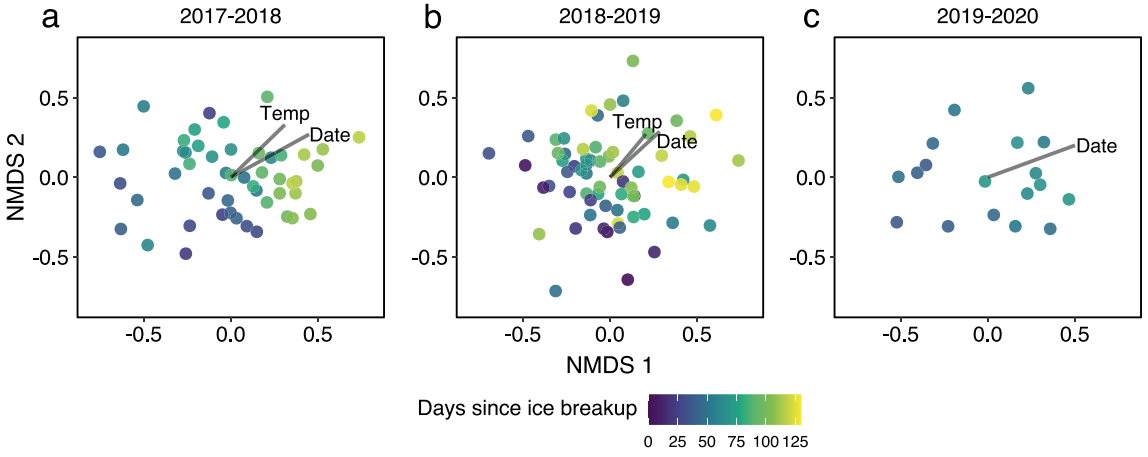

Fig. 6. Non-metric multidimensional scaling (NMDS) ordinations for zooplankton taxonomic composition at Stations B and E combined during the (a) 2017–2018, (b) 2018–2019, and (c) 2019–202 field seasons. Each point marks a sampling event. Vector direction represents the axis of maximal change for the environmental variable, and vector length indicates correlation strength with the environmental variable. 'Temp' refers to average temperature from 0–50 m, and 'Date' refers to the number of days since local sea-ice breakup (also indicated by color of the points). NMDS stress = 0.14–0.19, and individual values are provided in Table 2. The 2018–2019 data were fitted using 3 dimensions, and the third axis is presented in Fig. S1 in the Supplement

merteans (the latter 2 not significantly different between stations; Table 3) had intermediate central abundance dates between 16–22 January (Fig. 7a & Fig. S3 in the Supplement). Chaetognaths, *R. gigas*, *C. propinquus*, and *Oithona* spp. copepods typically increased in abundance from January until March (Fig. S4 in the Supplement) and had late mean central abundance dates ranging from 24 January to 1 February (Fig. 7a).

Pteropods and salps were both more abundant at Station E than at Station B (Table 3), and their seasonality was apparent in years when their densities were highest. In 2017–2018, the thecosome (shelled) pteropod *Limacina rangii* and its shell-less gymnosome pteropod predators both declined from early December until March (Fig. 9a). The salp *Salpa thompsoni* bloomed in 2020 and constituted 70% of the zooplankton dry weight on average during that year. Abundance of salp blastozooids peaked in the second half of January; conversely, salp oozooids were an order of magnitude more abundant in February vs. January at Station E (the only station sampled after 6 February 2020) (Fig. 9b).

Foraminifera were positively correlated with the local ice coverage at Station E (where glacial ice was rarer than at Station B) in 2018–2019 (Spearman's ρ = 0.62; $p < 0.001$) (Fig. S5 in the Supplement). Foraminifera abundance was highest upon local sea-ice break-up in November, and subsequent diminishing peaks coincided with periodic ice coverage in Decem-

Table 2. Results of regression analysis for non-metric multidimensional scaling (NMDS) ordinations from Stations B and E across each year of sampling. NA: not applicable

	NMDS 1	NMDS 2	NMDS 3	r^2	p
2017–2018 (n = 47; stress = 0.19)					
Days from ice breakup	0.86	0.51	NA	0.56	<0.0001
Temperature	0.68	0.73	NA	0.42	<0.0001
Chlorophyll *a*	−0.82	−0.57	NA	0.07	0.19
Tidal regime				0.01	0.73
Diurnal	0.03	−0.02	NA		
Semidiurnal	−0.03	0.00	NA		
2018–2019 (n = 65; stress = 0.17)					
Days from ice breakup	0.61	0.62	0.51	0.45	<0.0001
Temperature	0.56	0.74	0.37	0.28	<0.001
Chlorophyll *a*	−0.19	−0.43	0.88	0.09	0.13
Tidal regime				0.01	0.53
Diurnal	−0.05	−0.03	0.04		
Semidiurnal	0.03	0.02	−0.02		
2019–2020 (n = 18; stress = 0.14)					
Days from ice breakup	0.93	0.37	NA	0.59	0.002
Temperature	0.96	−0.27	NA	0.11	0.41
Chlorophyll *a*	−0.41	0.91	NA	0.02	0.84
Tidal regime				0.01	0.87
Diurnal	−0.03	−0.01	NA		
Semidiurnal	0.04	0.02	NA		

ber and January, until both foraminifera and sea ice became mostly absent in February and March.

4. DISCUSSION

4.1. Environmental context

Satellite-based sea-ice concentration suggests the timing of sea-ice retreat across the 3 yr of this study was consistent with the 1979–2020 average, with the dates of sea-ice retreat for the 50 × 50 km area near Palmer Station being within 9 d of the long-term mean (28 November ± 30 d SD). Though the timing of sea-ice retreat, historically, is more consistent than sea-ice advance (Stammerjohn et al. 2008), the date of sea-ice breakup varied by 27 d across 3 yr according to the first day of boat-based sampling. We posit increased light availability and the local onset of increased phytoplankton productivity more closely coincide with this boat-based metric rather than the spatially coarser satellite view.

The surface-intensified warming pattern we observed suggests that atmospheric forcing drove water-temperature patterns in each of the 3 yr of this study. Colder water temperatures in the 2018–2019 field season were coincident with below-average surface temperatures across the Antarctic Peninsula during January and February 2019 (Clem et al. 2020). The warmest water temperatures coincided with record-setting surface air temperatures along the Antarctic Peninsula in February 2020 (Xu et al. 2021). Therefore, nearshore ocean temperature in this study appears to reflect broader-scale atmospheric processes.

The seasonal progression of phytoplankton biomass accumulation followed known patterns, and chl *a* concentration was low to moderate for the study site. Shallow mixed layers relieve light limitation and allow rapid phytoplankton growth in nutrient-replete waters following sea-ice retreat (Mitchell & Holm-Hansen 1991, Nelson & Smith 1991). Wind and meltwater influence mixing and stratification to drive subsequent phytoplankton biomass peaks in late January and early March near Palmer Station (Car-

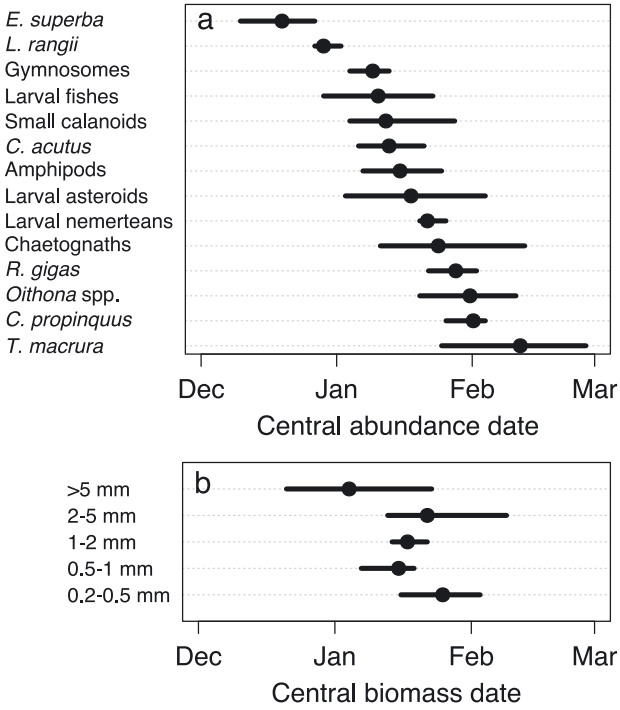

Fig. 7. Central date of zooplankton (a) taxonomic abundance and (b) size-fractionated biomass. Central dates were calculated individually for Stations B and E for the 2017–2018 and 2018–2019 field seasons. Therefore, the sample size n = 4 central dates for all taxa and size classes except for *L. rangii*, for which n = 3 due to absence. Black dots indicate the mean central date and error bars indicate the range across 2 years and 2 stations

Table 3. Zooplankton taxonomic abundance comparisons between Stations B and E. For taxa quantified from 700 µm net tows, n = 145 tows at Station B and n = 137 tows at Station E (except salps and euphausiids, for which n = 145 tows at both stations). For taxa quantified from 200 µm net tows, n = 69 tows at Station B and n = 65 tows at Station E. Paired Wilcoxon signed-rank tests were conducted using data collected on the same day at both stations. Daily station means were calculated for the 700 µm net when duplicate tows were available. Only data from the 2019–2020 field season were used in the paired Wilcoxon signed-rank test for *Salpa thompsoni* as it was predominantly absent in other years

Taxon	Station B mean ± SD (ind. m^{-3})	Station E mean ± SD (ind. m^{-3})	Wilcoxon signed-rank test		
			V	p	n (d)
700 µm net					
Euphausiids					
Euphausia superba	0.11 ± 0.63	0.043 ± 0.15	630	0.76	68
Thysanoessa macrura	0.015 ± 0.090	0.13 ± 0.29	543	0.025	68
Pteropods					
Limacina rangii	0.0075 ± 0.022	0.028 ± 0.054	65	<0.0001	68
Gymnosomes	0.0016 ± 0.0025	0.0024 ± 0.0047	609	0.085	68
Other					
Amphipods	0.0051 ± 0.0081	0.0040 ± 0.012	1371	0.006	68
Larval fishes	0.012 ± 0.025	0.0032 ± 0.0040	1593	<0.001	68
Salpa thompsoni blastozooids	0.052 ± 0.28	0.11 ± 0.45	5	0.039	9
200 µm net					
Copepods					
Oithona spp.	36.3 ± 32.4	21.8 ± 21.9	1462	0.002	63
Calanoides acutus	0.069 ± 0.061	0.043 ± 0.057	1568	<0.0001	63
Calanus propinquus	0.067 ± 0.072	0.041 ± 0.058	1439	<0.001	63
Rhincalanus gigas	0.047 ± 0.034	0.032 ± 0.047	1393	0.001	63
Small calanoids	6.9 ± 7.7	1.7 ± 4.1	1913	<0.0001	63
Other					
Chaetognaths	0.030 ± 0.031	0.0094 ± 0.014	1562	<0.0001	63
Larval asteroids	0.18 ± 0.24	0.17 ± 0.30	971	0.25	63
Larval nemerteans	0.40 ± 0.70	0.51 ± 1.0	521	0.086	63

valho et al. 2016, Nardelli et al. 2021). Mean December–February chl *a* concentration during each of the 3 study years (65–83 mg m^{-2}) was below the long-term mean for 1991–2012 (108 mg m^{-2}) (Saba et al. 2014). Therefore, while chl *a* was highest in our study during the summer of 2018–2019, phytoplankton biomass was only moderate in the context of the longer-term record.

4.2. Zooplankton biomass and size structure

Resource availability and predator–prey interactions drive the pattern of zooplankton biomass lagging behind phytoplankton biomass seasonally (Sommer et al. 2012). Recruitment of overwintering larvae (Atkinson 1991, Ward et al. 2012), ascension of seasonal vertical migrators (Atkinson & Shreeve 1995, La et al. 2019), and dampened diel vertical migration (Cisewski et al. 2010, Conroy et al. 2020) likely caused increased daytime zooplankton biomass following peaks in phytoplankton biomass accumulation. While meso- and macrozooplankton responded to phytoplankton growth, it is unlikely that, during 2017–2018 and 2018–2019, their grazing caused seasonal declines in phytoplankton biomass. Mean combined daily grazing by copepods, euphausiids, pteropods, and salps along the WAP is estimated at 0.5% of phytoplankton standing stock and 1.2% of daily primary productivity during summer (Bernard et al. 2012, Gleiber et al. 2016). However, salp blooms can lead to a daily grazing impact of up to 30% of phytoplankton standing stock (and 169% of primary productivity) (Bernard et al. 2012). Thus, the salp bloom in 2020 likely contributed to the low chl *a* conditions observed that year.

High concentration of biomass in the macrozooplankton size class (>2 mm) illustrates key characteristics of Antarctic zooplankton more broadly. The size of individual zooplankton is relatively large in polar regions due to low temperature, high oxygen concentration, and large phytoplankton (Brun et al. 2016, Brandão et al. 2021). And while subpolar regions have a much higher proportion of larger size classes of zooplankton compared to subtropical regions (e.g. Steinberg et al. 2008), the extreme 'top-heavy' zooplankton biomass conditions documented in this study and previously in the Scotia Sea (Tarling et al.

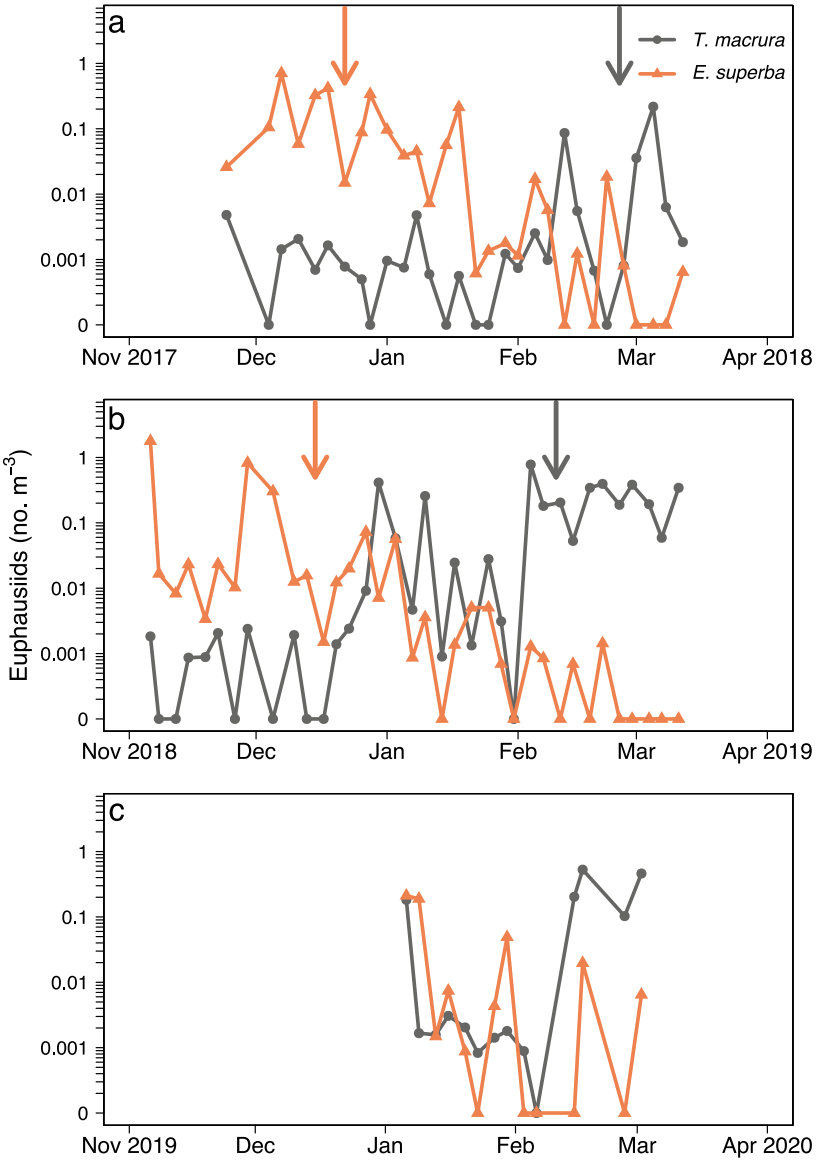

Fig. 8. Time series of mean *Euphausia superba* and *Thysanoessa macrura* abundance in (a) 2017–2018, (b) 2018–2019, and (c) 2019-2020 field seasons. Mean daily abundance was calculated from 700 µm net tows at Stations B and E combined (n = 1–4 tows per sampling day). Vertical arrows indicate the corresponding central abundance date for each species for the 2017–2018 and 2018–2019 field seasons. Note: mean plotted on logarithmic scale

2012) may be a distinct feature of the Southern Ocean. The inverted biomass distribution demonstrated here is likely possible due to high predator-to-prey size ratios and broad prey preferences (Woodson et al. 2018) characteristic of *Euphausia superba* and *Salpa thompsoni* (predator:prey ratios exceeding 10 000:1) (Schmidt & Atkinson 2016, Pauli et al. 2021, Stukel et al. 2021). Model simulations demonstrate the exceptional grazing and particle export impacts of large, long-lived macrozooplankton throughout the Southern Ocean (Le Quéré et al. 2016, Karakuş et al. 2021).

By repeatedly sampling at a high frequency over 3 yr, we demonstrate the patchiness of krill aggregations and ephemeral nature of salp blooms in contrast to the relatively homogenous distribution of mesozooplankton (dominated by copepods). As noted above, large taxa can have outsized roles in ecosystem-level processes, but these ecological impacts are limited in space and time while those of mesozooplankton are more consistent. For example, *Oithona* spp. copepods (dominant in 0.2–0.5 mm size class) may be the most productive zooplankton in the Southern Ocean due to their numerical abundance (Fransz & Gonzalez 1995), and calanoid copepods (dominant in 0.5–2 mm) are likely more productive than *E. superba* (Voronina 1998). Distinguishing multiple size classes of zooplankton is an effective way to model global ocean ecosystems (Le Quéré et al. 2016, Heneghan et al. 2020), and we suggest that regional studies attempt to resolve the distribution of zooplankton size classes at finer resolution.

4.3. Seasonal succession

Within each field season, days since sea-ice breakup and warming water temperatures were associated with changing zooplankton taxonomic composition. Chl *a* and tidal regime were not related to taxonomic structure. This suggests that (at our sampling resolution) advection and short-term phytoplankton changes were less important than a gradual restructuring of species composition as temperature increased after sea-ice breakup and throughout austral summer.

One component of seasonal succession was a transition to more omnivorous species. For example, the krill *E. superba* was more abundant in spring and occupies a lower trophic position than the krill species *Thysanoessa macrura* (Yang et al. 2021), which increased in abundance from spring into autumn. A similar transition occurred for copepods. The herbivorous *Calanoides acutus* peaked before the omnivorous and detritivorous *Calanus propinquus* and *Oithona*

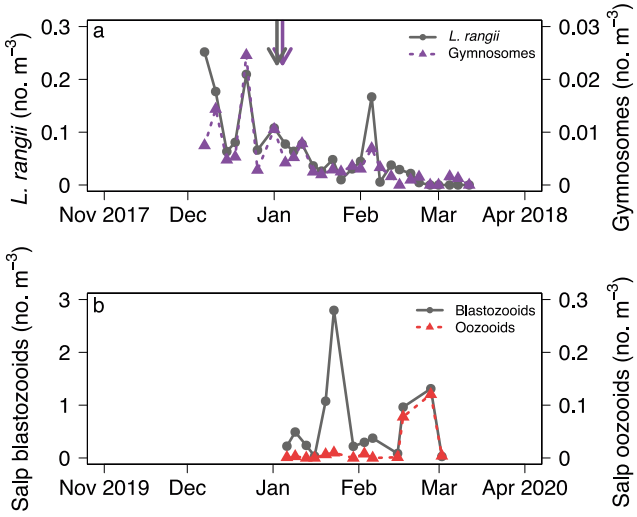

Fig. 9. Time series of pteropods and salps at Station E. (a) Thecosome (*Limacina rangii*) and gymnosome pteropods, and (b) the 2 life-history stages of the salp *Salpa thompsoni* (blastozooid 'aggregate' stage, and oozooid 'solitary' stage). Data are from the 2017–2018 field season for pteropods and from the 2019–2020 field season for salps. Mean daily abundance was calculated from 700 µm net tows (n = 1–2 tows per sampling day). Vertical arrows indicate the corresponding central abundance date for each pteropod group in panel a. Note different *y*-axis scales within and between plots

spp. copepods (Atkinson 1998). The copepod *Rhincalanus gigas* exhibited a bimodal seasonal distribution and is a generalist omnivore (Atkinson 1998), suggesting it takes advantage of different prey sources throughout the season. Carnivorous chaetognaths also had a bimodal abundance pattern and likely fed on different copepod prey throughout the seasonal succession (Hopkins & Torres 1989). The pteropod *Limacina rangii* largely relies on herbivory (Thibodeau et al. 2022) and decreased in abundance from spring into autumn. Carnivorous gymnosome pteropods were seasonally coupled with their *L. rangii* prey, as previously demonstrated at the interannual scale (Thibodeau et al. 2019).

In addition to differences in feeding ecology, reproductive timing and overwintering strategies help explain why some taxa were more abundant early in the seasonal cycle. Early spawning, recruitment, and seasonal vertical migration are characteristic for *C. acutus*, *R. gigas*, and *L. rangii* (Atkinson & Shreeve 1995, Thibodeau et al. 2020). A large portion of the small calanoids also followed this springtime recruitment or ascension pattern. Larval *E. superba* remain in surface waters during winter and recruit as juveniles in spring when they feed on phytoplankton throughout the day before initiating diel vertical migration in late summer (Nicol 2006, Nardelli et al. 2021). The seasonal decline in *E. superba* in our study may also be due to high predation mortality. The rapid rise in the density of larval fishes we observed following local sea-ice breakup allows for completion of larval development during the productive summer period when fishes feed on calanoid copepods (Kellermann 1989, Loeb et al. 1993). Foraminifera live within sea ice (Lipps & Krebs 1974, Spindler & Dieckmann 1986), and we found them to be abundant in the water column when sea ice was present. Few studies have focused on Antarctic foraminifera in recent decades (Bergami et al. 2009, Pinkerton et al. 2020), but the effects of a circumpolar release of foraminifera upon annual sea-ice retreat on both food web structure and biogeochemistry should be investigated.

A broad range of life-history strategies also result in patterns other than a spring maximum and seasonal decline. The seasonal increase in *C. propinquus* and *Oithona* spp. is likely tied to recruitment rather than a seasonal ascent. These copepods have a prolonged reproductive period and feed year-round rather than undergoing winter diapause (Metz 1995, Atkinson 1998, Pasternak & Schnack-Schiel 2001). Delayed recruitment likely explains occasional late-season increases in *R. gigas* and small calanoids. A horizontal migration may drive the seasonal increase of the krill *T. macrura*, a species which generally shifts southward and towards coastal waters at the end of summer (Nordhausen 1994, Loeb & Santora 2015). Persistent sampling of a *S. thompsoni* bloom through January and February allowed us to follow the stages of this species' complex life history. *S. thompsoni* blooms develop from asexual reproduction by a relatively small number of oozooids ('solitary' stage) that each release chains containing hundreds of blastozooids ('aggregate' stage; Loeb & Santora 2012), which were abundant in January. The blastozooids then reproduce sexually, resulting in increased oozooid abundance as the bloom progressed in February 2020. The oozooids then overwinter at depth (Loeb & Santora 2012) and begin the life cycle again the following summer. We observed the highest amphipod densities in 2020 (Fig. S2) during the salp bloom when amphipods (particularly *Vibilia* spp.) formed parasitic or commensal relationships within salps (Madin & Harbison 1977, Phleger et al. 2000).

Intermediate central abundance dates for larval asteroids and nemerteans reflect life-history traits of the dominant local species. The sea star *Odontaster validus* and ribbon worm *Parborlasia corrugatus* are abundant, well-studied species that spawn planktotrophic larvae, which may spend 5–6 mo in the

plankton (Pearse & Bosch 1986, Peck 1993). Both of these species spawn throughout the year, although reproductive output is concentrated in winter (Pearse et al. 1991, Stanwell-Smith et al. 1999). The minor fluctuations (rather than distinct seasonal trends) that we observed in larval abundance are likely due to multiple spawning pulses or advection. These larvae may feed on dissolved organic matter, bacteria, and detritus in addition to phytoplankton (Rivkin et al. 1986, Peck 1993), thus the lack of synchronization with phytoplankton biomass accumulation in our study supports previous work suggesting that larvae rely more upon increased phytoplankton productivity for growth and survival after settlement rather than when in the plankton (Bowden et al. 2009).

4.4. Phenological and long-term change

Phenological shifts (typically, earlier when warmer) are a fundamental response of marine plankton to climate variability and change (Mackas et al. 2012, Beaugrand & Kirby 2018). We documented ≥1 wk phenological shifts in the krill *E. superba* and *T. macrura*, *Oithona* spp. and small calanoid copepods, amphipods, chaetognaths, and larval fishes that coincided with a 2 wk earlier sea-ice breakup and onset of phytoplankton productivity. Temperature is the dominant driver of zooplankton phenology at lower latitudes (Ji et al. 2010, Mackas et al. 2012), but earlier accumulation occurred in the coldest year of our study. Thus, while seasonal warming likely influences taxonomic composition within each year, the timing of sea-ice breakup and increased phytoplankton productivity may drive interannual phenology shifts at the WAP.

Although some zooplankton taxa showed phenological responses to phytoplankton shifts, seasonal trophic mismatches remain possible. Phytoplankton phenology is commonly observed to shift faster than that of zooplankton in response to warming temperatures (Richardson 2008, Thackeray et al. 2016). The large copepods *C. acutus*, *R. gigas*, and *C. propinquus* exhibited limited phenological plasticity at Station B (<1 wk change in central abundance date between years), suggesting the spawning stages of these species may be more susceptible to trophic mismatches. However, direct evidence of decreased fitness due to seasonal mismatches is rare (Kharouba & Wolkovich 2020). Species inhabit areas along the WAP over which sea-ice duration varies by as much as 3 mo (Stammerjohn et al. 2008) and cope with changing environmental conditions via various physiological and behavioral responses such as diapause, vertical migration, and omnivory (Atkinson 1998, Conroy et al. 2020), that may preempt phenological responses (Beaugrand & Kirby 2018). Thus, flexible life history and feeding ecology can limit the risk of reproductive failure for zooplankton despite warming-induced trophic mismatches (Atkinson et al. 2015).

Our third field season captured conditions that are predicted to become more common as climate change progresses along the WAP. Warmer surface temperatures (Bracegirdle et al. 2020), reduced phytoplankton (particularly diatom) biomass (Brown et al. 2019), and more frequent salp blooms (Moline et al. 2004) are all hypothesized regional consequences of climate change. Copepod and krill abundances are positively related to phytoplankton productivity (Gleiber 2014, Steinberg et al. 2015), while warmer conditions favor pteropods (Thibodeau et al. 2019) and salps (Groeneveld et al. 2020). The substantial grazing impact of pteropods and salps (Bernard et al. 2012) may intensify competition among zooplankton species for their phytoplankton prey (Loeb et al. 1997), but the degree of competition depends upon feeding selectivity across species (Pauli et al. 2021, Stukel et al. 2021).

5. CONCLUSIONS

We documented substantial seasonal change in a coastal Antarctic zooplankton community over 3 yr with markedly different environmental conditions. Size and taxonomic composition shifted gradually after sea-ice breakup as the water column warmed each year. Zooplankton succession was exemplified by a switch of euphausiid species from *Euphausia superba* in spring to *Thysanoessa macrura* in late summer. Mesozooplankton biomass was relatively consistent compared to large seasonal and interannual fluctuations in macrozooplankton, which occasionally drove high biomass concentrations. Further assessment of the preserved sample collection produced by this study may provide valuable insights into species-specific dynamics for certain taxa (e.g. chaetognaths and small calanoid copepods) that were aggregated in our analysis. Such collections are an irreplaceable resource for assessing ecological shifts over time. Although we saw evidence for resilience, it remains unclear to what extent shifting phenology will drive population-level impacts and altered zooplankton composition as climate change progresses. Detecting such shifts will only be possible with sustained, coordinated observation.

Acknowledgements. This work was supported by the National Science Foundation Antarctic Organisms and Ecosystems Program (PLR-1440435 and OPP-2026045). M.I.T. was supported by the VIMS Research Experience for Undergraduates program (NSF OCE-1659656). Tide data were made available by the University of Wisconsin-Madison and Madison College AMRDC (NSF 1924730 and 1951603). Thank you to the Antarctic Support Contract personnel at Palmer Station for their scientific and logistical support. We thank Kharis Schrage, Andrew Corso, Ashley Hann, and Rachael Young for their field contributions to this project. Michael Gibson assisted with laboratory work. Sharon Stammerjohn, Oscar Schofield, Schuyler Nardelli, and Nicole Waite provided environmental data. Comments from Kim Bernard, David Johnson, Walker Smith, Mike Vecchione, and 3 anonymous reviewers improved this manuscript.

LITERATURE CITED

Amos AF (1993) RACER: The tides at Palmer Station. Antarct J US 28:162

Atkinson A (1991) Life cycles of *Calanoides acutus, Calanus simillimus* and *Rhincalanus gigas* (Copepoda: Calanoida) within the Scotia Sea. Mar Biol 109:79–91

Atkinson A (1998) Life cycle strategies of epipelagic copepods in the Southern Ocean. J Mar Syst 15:289–311

Atkinson A, Shreeve RS (1995) Response of the copepod community to a spring bloom in the Bellingshausen Sea. Deep Sea Res II 42:1291–1311

Atkinson A, Harmer RA, Widdicombe CE, McEvoy AJ and others (2015) Questioning the role of phenology shifts and trophic mismatching in a planktonic food web. Prog Oceanograph 137:498–512

Beaugrand G, Kirby RR (2018) How Do Marine Pelagic Species Respond to Climate Change? Theories and Observations. Annu Rev Mar Sci 10:169–197

Bergami C, Capotondi L, Langone L, Giglio F, Ravaioli M (2009) Distribution of living planktonic foraminifera in the Ross Sea and the Pacific sector of the Southern Ocean (Antarctica). Mar Micropaleontol 73:37–48

Bernard KS, Steinberg DK, Schofield OME (2012) Summertime grazing impact of the dominant macrozooplankton off the Western Antarctic Peninsula. Deep Sea Res I 62:111–122

Bernard KS, Cimino M, Fraser W, Kohut J and others (2017) Factors that affect the nearshore aggregations of Antarctic krill in a biological hotspot. Deep Sea Res I 126:139–147

Bowden DA, Clarke A, Peck LS (2009) Seasonal variation in the diversity and abundance of pelagic larvae of Antarctic marine invertebrates. Mar Biol 156:2033–2047

Bracegirdle TJ, Krinner G, Tonelli M, Haumann FA and others (2020) Twenty first century changes in Antarctic and Southern Ocean surface climate in CMIP6. Atmospheric Science Letters 21:e984

Brandão MC, Benedetti F, Martini S, Soviadan YD and others (2021) Macroscale patterns of oceanic zooplankton composition and size structure. Sci Rep 11:15714

Brown JH, Gillooly JF, Allen AP, Savage VM, West GB (2004) Toward a metabolic theory of ecology. Ecology 85: 1771–1789

Brown MS, Munro DR, Feehan CJ, Sweeney C, Ducklow HW, Schofield OM (2019) Enhanced oceanic CO_2 uptake along the rapidly changing West Antarctic Peninsula. Nat Clim Chang 9:678–683

Brun P, Payne MR, Kiørboe T (2016) Trait biogeography of marine copepods — an analysis across scales. Ecol Lett 19:1403–1413

Carvalho F, Kohut J, Oliver MJ, Sherrell RM, Schofield O (2016) Mixing and phytoplankton dynamics in a submarine canyon in the West Antarctic Peninsula. J Geophys Res Oceans 121:5069–5083

Cisewski B, Strass VH, Rhein M, Krägefsky S (2010) Seasonal variation of diel vertical migration of zooplankton from ADCP backscatter time series data in the Lazarev Sea, Antarctica. Deep Sea Res I 57:78–94

Clem KR, Barreira S, Fogt RL, Colwell S, Keller LM, Lazzara MA, Mikolajczyk D (2020) Atmospheric circulation and surface observations. In: Scambos T, Stammerjohn S (eds) State of the Climate in 2019. Antarctica and the Southern Ocean (Special Online Supplement). Bull Am Meteorol Soc 101:S293–S296

Conroy JA, Steinberg DK, Thibodeau PS, Schofield O (2020) Zooplankton diel vertical migration during Antarctic summer. Deep Sea Res I 162:103324

Dietrich K, Santora J, Reiss C (2021) Winter and summer biogeography of macrozooplankton community structure in the northern Antarctic Peninsula ecosystem. Prog Oceanogr 196:102610

Dinno A (2017) dunn.test: Dunn's test of multiple comparisons using rank sums. R package version 1.3.5. https://CRAN.R-project.org/package=dunn.test

Edwards M, Richardson AJ (2004) Impact of climate change on marine pelagic phenology and trophic mismatch. Nature 430:881–884

Fransz HG, Gonzalez SR (1995) The production of *Oithona similis* (Copepoda: Cyclopoida) in the Southern Ocean. ICES J Mar Sci 52:549–555

Froneman P, Pakhomov E, Perissinotto R, Laubscher R, McQuaid C (1997) Dynamics of the plankton communities of the Lazarev Sea (Southern Ocean) during seasonal ice melt. Mar Ecol Prog Ser 149:201–214

Gleiber MR (2014) Long-term change in copepod community structure in the Western Antarctic Peninsula: linkage to climate and implications for carbon cycling. MS thesis, College of William and Mary, Williamsburg, VA

Gleiber MR, Steinberg DK, Schofield OM (2016) Copepod summer grazing and fecal pellet production along the Western Antarctic Peninsula. J Plankton Res 38:732–750

Groeneveld J, Berger U, Henschke N, Pakhomov EA, Reiss CS, Meyer B (2020) Blooms of a key grazer in the Southern Ocean—an individual-based model of *Salpa thompsoni.* Prog Oceanogr 185:102339

Heneghan RF, Everett JD, Sykes P, Batten SD and others (2020) A functional size-spectrum model of the global marine ecosystem that resolves zooplankton composition. Ecol Modell 435:109265

Henley SF, Schofield OM, Hendry KR, Schloss IR and others (2019) Variability and change in the west Antarctic Peninsula marine system: research priorities and opportunities. Prog Oceanogr 173:208–237

Hopkins TL, Torres JJ (1989) Midwater food web in the vicinity of a marginal ice zone in the western Weddell Sea. Deep Sea Res A 36:543–560

Hunt BPV, Hosie GW (2006) The seasonal succession of zooplankton in the Southern Ocean south of Australia, part I: The seasonal ice zone. Deep Sea Res I 53:1182–1202

Janssen AW, Bush SL, Bednaršek N (2019) The shelled pteropods of the northeast Pacific Ocean (Mollusca: Heterobranchia, Pteropoda). Zoosymposia 13:305–356

Ji R, Edwards M, Mackas DL, Runge JA, Thomas AC (2010)

Marine plankton phenology and life history in a changing climate: current research and future directions. J Plankton Res 32:1355–1368

Karakuş O, Völker C, Iversen M, Hagen W, Gladrow DW, Fach B, Hauck J (2021) Modeling the impact of macrozooplankton on carbon export production in the Southern Ocean. J Geophys Res Oceans 126:e2021JC017315

Kellermann A (1989) The larval fish community in the zone of seasonal ice cover and its seasonal and interannual variability. Arch FischWiss 39:89–109

Kenitz KM, Visser AW, Mariani P, Andersen KH (2017) Seasonal succession in zooplankton feeding traits reveals trophic trait coupling. Limnol Oceanogr 62:1184–1197

Kharouba HM, Wolkovich EM (2020) Disconnects between ecological theory and data in phenological mismatch research. Nat Clim Chang 10:406–415

Kim H, Doney SC, Iannuzzi RA, Meredith MP, Martinson DG, Ducklow HW (2016) Climate forcing for dynamics of dissolved inorganic nutrients at Palmer Station, Antarctica: An interdecadal (1993-2013) analysis. J Geophys Res Biogeosci 121:2369–2389

Kim H, Ducklow HW, Abele D, Ruiz Barlett EM and others (2018) Inter-decadal variability of phytoplankton biomass along the coastal West Antarctic Peninsula. Philos Trans A Math Phys Eng Sci 376:20170174

Kiørboe T, Visser A, Andersen KH (2018) A trait-based approach to ocean ecology. ICES J Mar Sci 75:1849–1863

La HS, Park K, Wåhlin A, Arrigo KR and others (2019) Zooplankton and micronekton respond to climate fluctuations in the Amundsen Sea polynya, Antarctica. Sci Rep 9:10087

Le Quéré C, Buitenhuis ET, Moriarty R, Alvain S and others (2016) Role of zooplankton dynamics for Southern Ocean phytoplankton biomass and global biogeochemical cycles. Biogeosciences 13:4111–4133

Lipps JH, Krebs WN (1974) Planktonic foraminifera associated with Antarctic sea ice. J Foraminiferal Res 4:80–85

Litchman E, Ohman MD, Kiørboe T (2013) Trait-based approaches to zooplankton communities. J Plankton Res 35:473–484

Loeb VJ, Santora JA (2012) Population dynamics of *Salpa thompsoni* near the Antarctic: growth rates and interannual variations in reproductive activity (1993–2009). Progr Oceanogr 96:93–107

Loeb VJ, Santora JA (2015) Climate variability and spatiotemporal dynamics of five Southern Ocean krill species. Prog Oceanogr 134:93–122

Loeb VJ, Kellermann AK, Koubbi P, North AW, White MG (1993) Antarctic larval fish assemblages: a review. Bull Mar Sci 53:416–449

Loeb V, Siegel V, Holm-Hansen O, Hewitt R, Fraser W, Trivelpiece W, Trivelpiece S (1997) Effects of sea-ice extent and krill or salp dominance on the Antarctic food web. Nature 387:897–900

Mackas DL, Greve W, Edwards M, Chiba S and others (2012) Changing zooplankton seasonality in a changing ocean: Comparing time series of zooplankton phenology. Prog Oceanogr 97–100:31–62

Madin LP, Harbison GR (1977) The associations of Amphipoda Hyperiidea with gelatinous zooplankton — I. Associations with Salpidae. Deep Sea Res 24:449–463

Metz C (1995) Seasonal variation in the distribution and abundance of *Oithona* and *Oncaea* species (Copepoda, Crustacea) in the southeastern Weddell Sea, Antarctica. Polar Biol 15:187–194

Minchin PR (1987) An evaluation of the relative robustness of techniques for ecological ordination. Vegetatio 69:89–107

Mitchell BG, Holm-Hansen O (1991) Observations of modeling of the Antartic phytoplankton crop in relation to mixing depth. Deep Sea Res A 38:981–1007

Moline MA, Claustre H, Frazer TK, Schofield O, Vernet M (2004) Alteration of the food web along the Antarctic Peninsula in response to a regional warming trend. Glob Change Biol 10:1973–1980

Nardelli SC, Cimino MA, Conroy JA, Fraser WR, Steinberg DK, Schofield O (2021) Krill availability in adjacent Adélie and gentoo penguin foraging regions near Palmer Station, Antarctica. Limnol Oceanogr 66:2234–2250

Nelson DM, Smith WO Jr (1991) Sverdrup revisited: critical depths, maximum chlorophyll levels, and the control of Southern Ocean productivity by the irradiance-mixing regime. Limnol Oceanogr 36:1650–1661

Nicol S (2006) Krill, currents, and sea ice: *Euphausia superba* and its changing environment. Bioscience 56:111–120

Nordhausen W (1994) Winter abundance and distribution of *Euphausia superba, E. crystallorophias*, and *Thysanoessa macrura* in Gerlache Strait and Crystal Sound, Antarctica. Mar Ecol Prog Ser 109:131–142

Oksanen J, Blanchet FG, Friendly M, Kindt R and others (2020) vegan: Community Ecology Package. R package version 2.5-7. https://CRAN.R-project.org/package=vegan

Oliver MJ, Irwin A, Moline MA, Fraser W, Patterson D, Schofield O, Kohut J (2013) Adélie penguin foraging location predicted by tidal regime switching. PLOS ONE 8:e55163

Pasternak AF, Schnack-Schiel SB (2001) Feeding patterns of dominant Antarctic copepods: an interplay of diapause, selectivity, and availability of food. Hydrobiologia 453:25–36

Pauli NC, Metfies K, Pakhomov EA, Neuhaus S and others (2021) Selective feeding in Southern Ocean key grazers — diet composition of krill and salps. Commun Biol 4:1

Pearse JS, Bosch I (1986) Are the feeding larvae of the commonest Antarctic asteroid really demersal? Bull Mar Sci 39:477–484

Pearse JS, McClintock JB, Bosch I (1991) Reproduction of Antarctic benthic marine invertebrates: tempos, modes, and timing. Am Zool 31:65–80

Peck LS (1993) Larval development in the Antarctic nemertean *Parborlasia corrugatus* (Heteronemertea: Lineidae). Mar Biol 116:301–310

Phleger CF, Nelson MM, Mooney B, Nichols PD (2000) Lipids of Antarctic salps and their commensal hyperiid amphipods. Polar Biol 23:329–337

Pinkerton MH, Décima M, Kitchener JA, Takahashi KT, Robinson KV, Stewart R, Hosie GW (2020) Zooplankton in the Southern Ocean from the continuous plankton recorder: Distributions and long-term change. Deep Sea Res I 162:103303

Postel L, Fock H, Hagen W (2000) Biomass and abundance. In: Harris R, Wiebe P, Lenz J, Skjoldal HR, Huntley M (eds) ICES zooplankton methodology manual. Academic Press, London, p 83–192

R Core Team (2021) R: A language and environment for statistical computing. R Foundation for Statistical Computing, Vienna

Richardson AJ (2008) In hot water: zooplankton and climate change. ICES J Mar Sci 65:279–295

Rivkin RB, Bosch I, Pearse JS, Lessard EJ (1986) Bacterivory: a novel feeding mode for asteroid larvae. Science 233: 1311–1314

Rykaczewski RR, Checkley DM (2008) Influence of ocean winds on the pelagic ecosystem in upwelling regions. Proc Natl Acad Sci USA 105:1965–1970

Saba GK, Fraser WR, Saba VS, Iannuzzi RA and others (2014) Winter and spring controls on the summer food web of the coastal West Antarctic Peninsula. Nat Commun 5:4318

Schmidt K, Atkinson A (2016) Feeding and food processing in antarctic krill (*Euphausia superba* Dana). In: Siegel V (ed) Biology and ecology of Antarctic krill. Advances in polar ecology. Springer, Cham, p 175–224

Schnack-Schiel SB (2001) Aspects of the study of the life cycles of Antarctic copepods. In: Lopes RM, Reid JW, Rocha CEF (eds) Copepoda: developments in ecology, biology and systematics. Springer, Dordrecht, p 9–24

Schofield O, Saba G, Coleman K, Carvalho F and others (2017) Decadal variability in coastal phytoplankton community composition in a changing West Antarctic Peninsula. Deep Sea Res I 124:42–54

Sommer U, Adrian R, De Senerpont Domis L, Elser JJ and others (2012) Beyond the Plankton Ecology Group (PEG) model: Mechanisms driving plankton succession. Annu Rev Ecol Evol Syst 43:429–448

Spindler M, Dieckmann GS (1986) Distribution and abundance of the planktic foraminifer *Neogloboquadrina pachyderma* in sea ice of the Weddell Sea (Antarctica). Polar Biol 5:185–191

Stamieszkin K, Pershing AJ, Record NR, Pilskaln CH, Dam HG, Feinberg LR (2015) Size as the master trait in modeled copepod fecal pellet carbon flux. Limnol Oceanogr 60:2090–2107

Stammerjohn SE, Martinson DG, Smith RC, Iannuzzi RA (2008) Sea ice in the western Antarctic Peninsula region: Spatio-temporal variability from ecological and climate change perspectives. Deep Sea Res II 55:2041–2058

Stanwell-Smith D, Peck LS, Clarke A, Murray AWA, Todd CD (1999) The distribution, abundance and seasonality of pelagic marine invertebrate larvae in the maritime Antarctic. Philos Trans R Soc B 354:471–484

Steinberg DK, Cope JS, Wilson SE, Kobari T (2008) A comparison of mesopelagic mesozooplankton community structure in the subtropical and subarctic North Pacific Ocean. Deep Sea Res II 55:1615–1635

Steinberg DK, Ruck KE, Gleiber MR, Garzio LM and others (2015) Long-term (1993–2013) changes in macrozooplankton off the Western Antarctic Peninsula. Deep Sea Res I 101:54–70

Stukel MR, Décima M, Selph KE, Gutiérrez-Rodríguez A (2021) Size-specific grazing and competitive interactions between large salps and protistan grazers. Limnol Oceanogr 66:2521–2534

Tarling GA, Stowasser G, Ward P, Poulton AJ and others (2012) Seasonal trophic structure of the Scotia Sea pelagic ecosystem considered through biomass spectra and stable isotope analysis. Deep Sea Res II 59-60:222–236

Thackeray SJ, Henrys PA, Hemming D, Bell JR and others (2016) Phenological sensitivity to climate across taxa and trophic levels. Nature 535:241–245

Thibodeau PS, Steinberg DK, Stammerjohn SE, Hauri C (2019) Environmental controls on pteropod biogeography along the Western Antarctic Peninsula. Limnol Oceanogr 64:S240–S256

Thibodeau PS, Steinberg DK, McBride CE, Conroy JA, Keul N, Ducklow HW (2020) Long-term observations of pteropod phenology along the Western Antarctic Peninsula. Deep Sea Res I 166:103363

Thibodeau PS, Song B, Moreno CM, Steinberg DK (2022) Feeding ecology and microbiome of the pteropod *Limacina helicina antarctica.* Aquat Microb Ecol 88:19–24

Visser AW, Brun P, Chakraborty S, Dencker TS and others (2020) Seasonal strategies in the world's oceans. Prog Oceanogr 189:102466

Voronina NM (1998) Comparative abundance and distribution of major filter-feeders in the Antarctic pelagic zone. J Mar Syst 17:375–390

Ward P, Atkinson A, Tarling G (2012) Mesozooplankton community structure and variability in the Scotia Sea: a seasonal comparison. Deep Sea Res II 59-60:78–92

Woodson CB, Schramski JR, Joye SB (2018) A unifying theory for top-heavy ecosystem structure in the ocean. Nat Commun 9:23

Xu M, Yu L, Liang K, Vihma T, Bozkurt D, Hu X, Yang Q (2021) Dominant role of vertical air flows in the unprecedented warming on the Antarctic Peninsula in February 2020. Commun Earth Environ 2:1–9

Yang G, Atkinson A, Hill SL, Guglielmo L, Granata A, Li C (2021) Changing circumpolar distributions and isoscapes of Antarctic krill: Indo-Pacific habitat refuges counter long-term degradation of the Atlantic sector. Limnol Oceanogr 66:272–287

Editorial responsibility: Shin-ichi Uye, Higashi-Hiroshima, Japan
Reviewed by: G. A. Tarling and 2 anonymous referees

Submitted: April 29, 2022
Accepted: January 26, 2023
Proofs received from author(s): February 20, 2023